Characteristic Interfacial Structure behind a Rapidly Moving Contact Line

Mengfei He and Sidney R. Nagel
Department of Physics, The James Franck and Enrico Fermi Institutes, The University of Chicago, Chicago, Illinois 60637, USA

(Received 31 July 2018; revised manuscript received 4 October 2018; published 10 January 2019)

In forced wetting, a rapidly moving surface drags with it a thin layer of trailing fluid as it is plunged into a second fluid bath. Using high-speed interferometry, we find characteristic structure in the thickness of this layer with multiple thin flat triangular structures separated by much thicker regions. These features, depending on liquid viscosity and penetration velocity, are robust and occur in both wetting and dewetting geometries. Their presence clearly shows the importance of motion in the transverse direction. We present a model using the assumption that the velocity profile is robust to thickness fluctuations that gives a good estimate of the gap thickness in the thin regions.

DOI: 10.1103/PhysRevLett.122.018001

Introduction.—A solid entrains surrounding air along with its moving surface when it is pushed rapidly into a liquid bath. In this process, known as "forced wetting," a three-phase contact line between the substrate, air, and liquid is forced to move across the surface of the solid. If the penetration velocity is high enough, the contact line distorts downwards to create a pocket of air.

When the substrate velocity U is low, the contact line remains approximately level with the liquid surface. At higher velocity, the line distorts and evolves towards a steady-state "V" shape [1–3], shown schematically in Fig. 1(a). The top row of Fig. 1(b) shows images, spaced 100 ms apart, of the transient evolution to this shape. The first frame shows the contact line immediately after a planar substrate starts to move at fixed velocity into a liquid bath; the next images show the development towards the steady-state V shown in the last frame.

These images, taken with white light, show the lateral evolution of the contact line but provide no information about the *thickness* of the air gap at different points across its surface. We obtain such information from interference fringes, which are visible when the optical path across the gap is less than the coherence length of the light. In the bottom panel of Fig. 1(b), interference fringes appear for thicknesses less than ≈ 30 μm. These images reveal unexpected structure in the gap thickness that was not visible in the top panel.

As the contact line evolves, the air gap is thick near the edge and becomes thin and extremely flat in the center. This flatness can be ascertained because over regions of approximately 5 mm in width there are only two fringes. These correspond to equal-height contours, with a difference in thickness between successive bright fringes of ≈ 0.32 μm. Once the contact line has formed the V shape,

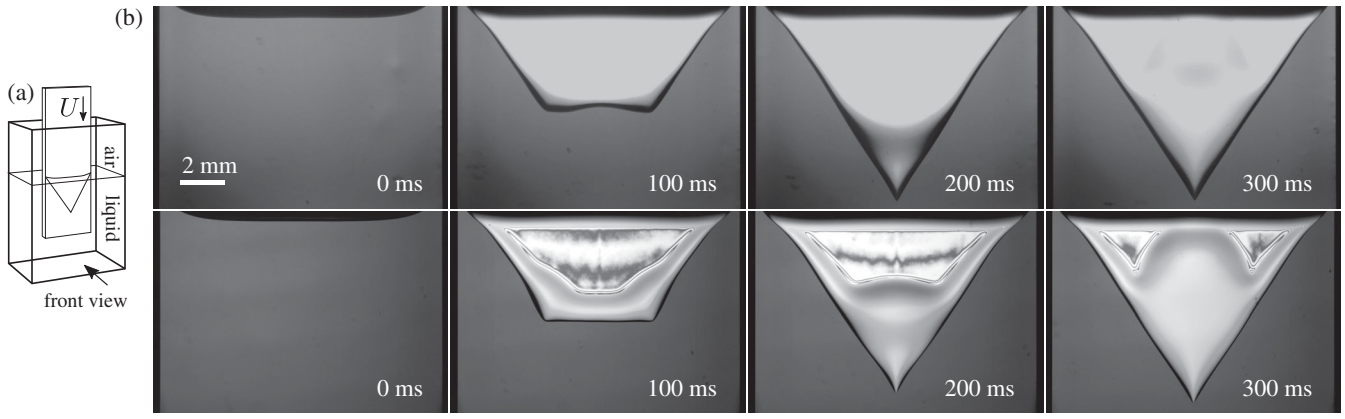

FIG. 1. (a) Schematic showing the V-shaped steady-state contact line as viewed from the front. (b) Images during the evolution of the V shape spaced 100 ms apart. A 12.7 mm wide tape travels vertically into a water-glycerol mixture of viscosity, $\eta = 226$ cP, at $U = 130$ mm/s. Top row: Images using a white light. Bottom row: Images using red light of coherence length 60 μm. Interference patterns appear where the air pocket is thinner than 60 μm/2 = 30 μm.

the air gap continues to evolve until it reaches a steady shape shown in the last frame; at that point the air pocket has two very flat triangular structures that are symmetrically placed in the upper corners of the gap separated by an intervening thicker region.

These features are very robust. They appear regardless of the solid material (e.g., metal or plastic) and the fluid viscosity; they appear if the air is replaced by a second liquid. More surprisingly, similar structures appear in dewetting experiments where the liquid drains from the substrate as it is withdrawn from the bath.

We measured the dependence of the gap dimensions on the liquid viscosity, substrate width, and penetration velocity. The absolute thickness at different points in the gap were measured in order to characterize the three-dimensional structure of the air pocket.

Methods.—In our experiments, we used flexible Mylar tape as the solid substrate. The tape was held vertically as it was forced into (wetting) or pulled out of (dewetting) the bath. Vibrations and twist were minimized by supports located along the path of the tape. These and the chamber walls were kept distant from the air pocket to avoid any interactions [4,5]. Except where specifically stated otherwise, the tape width was 12.7 mm. In each run, the tape velocity U was held constant at speeds between 50 and 1000 mm/s.

The liquid bath consisted of water-glycerol mixtures whose viscosity, η_{out}, could be tuned between different runs by varying the relative concentration of the components: 26 cP $\leq \eta_{\text{out}} \leq$ 572 cP. In order to check whether the structure of the gap was robust to the type of entrained fluid, we also replaced the air by a silicon oil of viscosity 0.65 cP. The interfacial tension γ and density ρ were measured for different mixtures to be between 53 and 66 mN/m and between 1.21 and 1.25 g/cm^3, respectively.

The absolute thickness $H(x, z)$ of the air gap at different points on the surface (x, z) was measured using high-speed interferometric imaging [6] from multiple wavelengths of light simultaneously (see Supplemental Material [7]) [8–10]. Once the thickness of the thin regions is known, the thickness of the gap in the thicker regions can be measured by counting fringes from a laser.

Role of viscosity and evolution to steady state.—The V shape of the steady-state contact line was quantitatively interpreted by Blake and Ruschak [3] in terms of a maximum contact-line velocity U_{max} with which the liquid can wet the solid. When $U > U_{\text{max}}$, the contact line is forced to tilt by an angle ϕ so that the normal velocity of the contact line does not surpass this threshold:

$$U \cos\phi = U_{\text{max}}. \tag{1}$$

Figure 2(a) shows $(\cos\phi)^{-1}$ versus U for liquids of different viscosities, η_{out}. [Because of growing contact-line fluctuations as U decreases towards U_{max}, our data do not extend below the dashed line, $(\cos\phi)^{-1} \approx 1.3$.] Figure 2(b) shows that U_{max} determined from Eq. (1) varies as

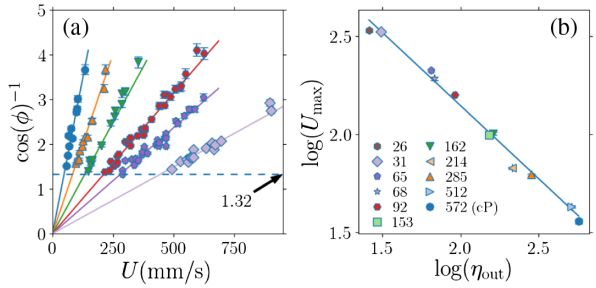

FIG. 2. (a) $(\cos\phi)^{-1}$ versus velocity U for water-glycerol mixtures with viscosities between 26 and 572 cP. Solid lines: least-square fits to Eq. (1). (b) U_{max} extracted from (a), versus η_{out}. Solid line: $U_{\text{max}} \sim \eta_{\text{out}}^{-0.75}$.

$$U_{\text{max}} \sim \eta_{\text{out}}^{-0.75\pm0.03}. \tag{2}$$

This exponent is similar to that found in earlier works [1,2,11–15], but is larger than the value (between 1/3 and 1/2) suggested by Marchant *et al.* [16].

Structure in the air gap.—The last image of Fig. 1(b) shows there is steady state structure in the thickness of the air gap $H(x, z)$. Most striking is the unexpected appearance of two flat triangular shapes in the upper corners of the last image. Figure 3 shows the tip separation W and the vertical span of the triangular regions L, as indicated in the insets. W saturates at large velocity U, suggesting it is determined by $\sqrt{\gamma/\rho g}$ (balance of buoyancy and surface tension). The slope of L versus U increases with increasing bath viscosity.

An average thickness of the air gap was previously estimated to be between 0.05 and 0.9 μm (e.g., see Refs. [1,17]); in the case of a plunging liquid jet (instead of plunging solid) it was measured to be several microns [18]. No structure within the gap was reported. However, Fig. 4(a) shows two profiles along the z direction of $H(x, z)$ obtained from the multiwavelength interference method described in the Supplemental Material [7]. The profiles are far from uniform; using only the average value is

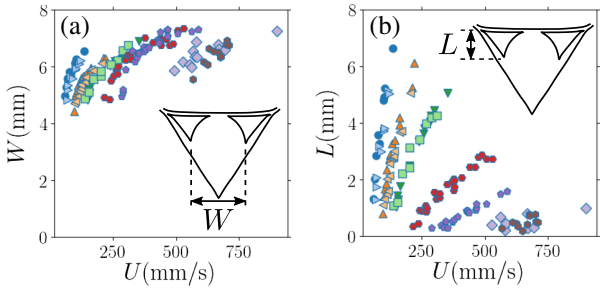

FIG. 3. Lateral geometry of thin structures in the air gap versus substrate velocity U. (a) Distance between tips W versus U, and (b) vertical span L versus U. W and L are shown in the insets.

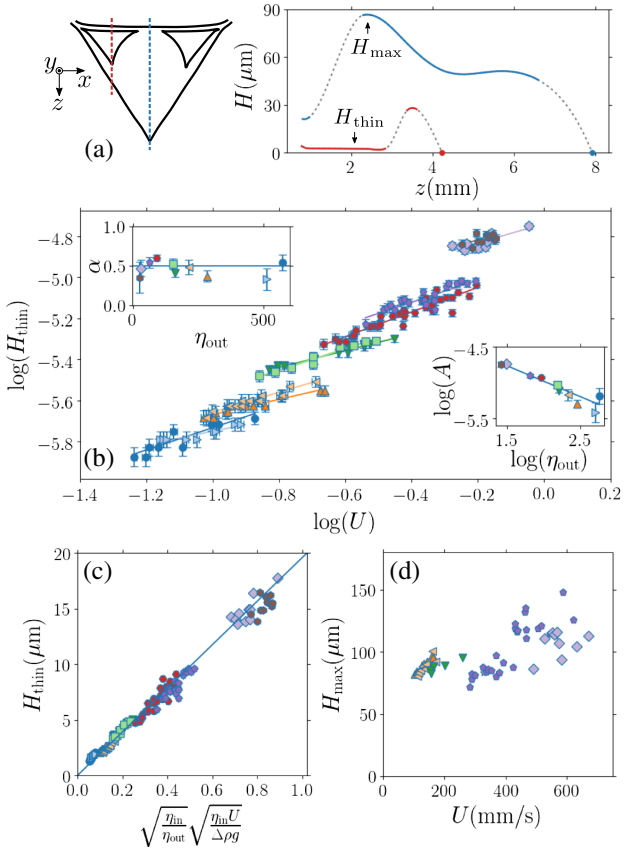

FIG. 4. Thickness of air gap. (a) Profiles of the gap thickness, as shown in the schematic (for $U \approx 120$ mm/s; $\eta_{out} \approx 200$ cP) along the thin triangular regions (red) and the center of the air gap where the thickness is maximum (blue). The solid lines are measurements and dashed lines are interpolations. Note the extremely thin flat section of the profile through the triangular region. (b) Thickness of the thin triangular regions measured at their centers H versus U. Lines show fits for $H_{thin} \propto AU^{\alpha}$. Upper inset: α versus η_{out}. The average $\langle\alpha\rangle \approx 0.46 \pm 0.03$. Lower inset: A versus η_{out}. Line shows fit $A \propto \eta_{out}^{-0.43}$. (c) Data collapsed to Eq. (8). (d) Thickness at thickest point of the gap H_{max} versus U.

misleading since it misses the complex structure. Figure 4(b) shows H_{thin}, the absolute gap thickness in the center of the triangular regions, versus U. These regions are extremely flat with a height variation of only $\Delta H_{thin} \approx 0.1 \sim 0.7$ μm depending on the outer fluid viscosity. As one might naively expect, H_{thin} increases with increasing penetration velocity. Each data set starts only when $U > U_{max}$ [from Fig. 2(b)]; thus as η_{out} increases, the data range shifts to lower velocities.

The data for different values of η_{out} *do not* fall on top of one another but splay out and are roughly parallel to one another. We fit each data set to the form: $H_{thin} = AU^{\alpha}$. The insets in Fig. 4(b) show the least-square fits of the parameters α and A versus η_{out}. The upper inset shows that the average $\alpha = 0.46 \pm 0.03$. This is significantly different from $\alpha = 2/3$ given by the Landau-Levich-Derjaguin theory for the *deposition* of a liquid layer on a substrate pulled out of a bath [19,20]. The lower inset shows $A \propto \eta_{out}^{\beta}$ with best-fit exponent $\beta = -0.43 \pm 0.07$ (solid line). This suggests

$$H_{thin} \propto U^{0.46\pm0.03}\eta_{out}^{-0.43\pm0.07}. \tag{3}$$

In order to understand this behavior, we model the air flow within the gap. Because of the stationary contact line, the total flux of air must be zero; any air that is entrained by the substrate must return to the surface. This is different from the case of deposition without a contact line [19,20].

Huh and Scriven [21] treated the case where there is no lateral flow so that the geometry is a two-dimensional wedge with a fluid-substrate contact angle θ. However, in forced wetting, with the V shape, there is clearly transverse flow. The central, thick part of the gap can accommodate the return of the entrained air so that in the thin triangular regions there need not be any return flow. In those regions, the entrained air can escape by flowing downwards towards the contact line and then sideways towards the central thicker part of the gap. This is different from the flow proposed by Severtson and Aidun [22] who did not observe the thin triangular regions.

We assume that the velocity of the liquid-air interface, U_I, does not vary significantly across the surface and can be approximated by the two-dimensional results of Huh and Scriven:

$$U_I = \zeta U \approx \left(1 - D(\theta)\frac{\eta_{in}}{\eta_{out}}\right)U, \tag{4}$$

where η_{in} is the *inner* fluid viscosity (air in our case). The first order expansion of ζ in terms of η_{in}/η_{out} is valid near $\theta \approx 3°$ over our experimental range of $\eta_{in}/\eta_{out} \ll 1$. (See Supplemental Material [7] for more details).

In the thin regions, where the liquid interface is nearly vertical, the buoyancy force is balanced by the viscous forces in the inner fluid: $\eta_{in}\partial^2 u(y)/\partial y^2 = \Delta\rho g$, where y is in the horizontal direction perpendicular to the substrate surface, flow is in the z direction [see Fig. 4(a)], and $\Delta\rho g$ is the buoyancy force. Using the boundary conditions at the substrate $u(y = 0) = U$ and at the liquid-liquid interface $u(y = H_{thin}) = U_I$ we find,

$$u = \frac{\Delta\rho g}{2\eta_{in}}y^2 - By + U \tag{5}$$

$$\text{with} \quad B = \frac{(1-\zeta)U}{H_{thin}} + \frac{\Delta\rho g}{2\eta_{in}}H_{thin}. \tag{6}$$

Given an arbitrary H_{thin} there is a solution satisfying both boundary conditions. $B(H_{thin})$ determines the flow profile. We note that infinitesimal fluctuations of H_{thin} change B except at its extremum: $dB/dH_{thin} = 0$. For this solution, not only is B independent of H_{thin}, but the profile has zero

slope, $\partial u/\partial y = 0$ at the fluid-fluid interface (see Supplemental Material [7]); fluctuations in H_{thin} only minimally perturb the flow in the gap. We argue that the system selects this solution because it is the most robust and invariant to such fluctuations that would otherwise disrupt the flow profile. Setting $dB/dH_{\text{thin}} = 0$ gives

$$H_{\text{thin}} = \left(2(1-\zeta)\frac{\eta_{\text{in}}}{\Delta\rho g}U\right)^{\frac{1}{2}}. \tag{7}$$

We note that this is the same solution as is obtained by minimizing the total dissipation in the air in the thin part of the gap: $D_{\text{diss}} \propto \int_0^{H_{\text{thin}}} \eta_{\text{in}}(\partial u/\partial y)^2 dy$ (see Supplemental Material [7] for more discussion).

Inserting Eq. (4) for ζ leads to

$$H_{\text{thin}} = (2D(\theta))^{\frac{1}{2}}\left(\frac{\eta_{\text{in}}}{\eta_{\text{out}}}\right)^{\frac{1}{2}}\left(\frac{\eta_{\text{in}}U}{\Delta\rho g}\right)^{\frac{1}{2}}. \tag{8}$$

A characteristic length scale $(\eta_{\text{in}}U/\Delta\rho g)^{1/2}$ emerges and is independent of the interfacial tension γ [23].

Comparing Eq. (8) to our data in Fig. 4(c) shows excellent agreement with $D(\theta) \approx 193$, corresponding to $\theta = 2.7°$. To see if $\theta = 2.7°$ is reasonable in our experiment, we measure H_{max}, the maximum thickness of the pocket near the center of the V shape. Figure 4(d) shows that H_{max} is typically $\sim 100\ \mu$m, which is more than an order of magnitude larger than H_{thin}, and has large fluctuations. From H_{max} and the dimensions of the V shape, we estimate θ as the *average* slope of the overall pocket to be between 1° and 4°. Alternatively, the *local* slope at the contact line, estimated from the interpolations in Fig 4(a), gives a consistent value $\theta \approx 3.0°$. Thus, this model for the air flow in the thin regions is in quantitative agreement with our data.

When the substrate width is varied, the number of thin regions in the air gap varies but leaves the distance W between them roughly constant. This suggests that the saturation width shown in Fig. 3(a) is independent of the substrate width. Figure 5(a) shows an image of such an entrained layer for a 25.4 mm wide tape (i.e., twice as wide as was used in the data shown above) with more thin-thick alternations across the tape surface. Similar thin triangles appear if the air is replaced by another fluid as shown in Fig. 5(b) where a 12.7 mm tape moves between a 0.65 cP silicone oil and a 60 cP water-glycerol mixture. Two thin triangular regions appear in the upper corners of the V. If we reverse the direction of U, so that the solid emerges from the bath and the liquid dewets the substrate, a liquid film forms with three thin regions (now near the bottom) as shown in Fig. 5(c). Rimlike structure behind the contact line in the longitudinal direction was previously seen in dewetting [24–27], but no transverse thickness modulation was reported. As with forced wetting, increasing the substrate width produces more thin-thick alternations while leaving the distance W between thin parts roughly constant. Thus these thin triangular regions are a robust feature under both wetting and dewetting conditions.

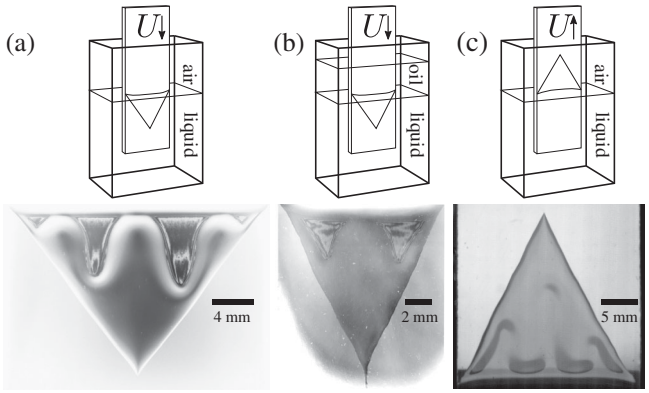

FIG. 5. Robustness of structure for wetting and dewetting geometries as shown in schematics. (a) A wide 25.4 mm tape moving from air into an 150 cP water-glycerol bath showing four thin regions. (b) A 0.65 cP silicone oil (replacing air) above a 60 cP water-glycerol mixture. A tape of width 12.7 mm shows two thin triangular regions. (c) A tape of width 25.4 mm pulled out of a water bath into air shows three thin regions. Gray scale inverted for clarity in (a) and (b).

The scalings we found for wetting need not apply to dewetting because the expansion in Eq. (4) is generally not valid when $\eta_{\text{in}}/\eta_{\text{out}} > 1$. However, our study suggests that the presence of a contact line may affect the interfacial velocity even in dewetting where the Landau-Levich-Derjaguin theory had been assumed to hold.

Summary.—We have found an unexpected characteristic entrained layer in forced-wetting and dewetting experiments. This structure, consisting of flat thin sections alternating with thick pockets, is stable and is controlled by viscosity contrast between the inner and outer fluids, the penetration velocity and width of the substrate.

For thin film problems such as gravitational flows, liquid films in rotating cylinders (i.e., printer's instability), spinning drops, and circular hydraulic jumps, the instability along the direction perpendicular to the general motion of the fluid has been observed and analyzed [28–34]. On the other hand, many attempts to understand wetting ignore motion transverse to the velocity of the substrate [35]. Such a simplification reduces the problem to a two-dimensional geometry. While effective in describing the onset of the forced-wetting transition [25,26,36–40], such analyses exclude the three-dimensional structures that emerge at later stages. Our experiments show that a pure two-dimensional analysis is no longer adequate in the steady state. The persistent thin triangular gaps separated by a thick region reflects the nonuniformity of the back flow of the entrained fluid. This suggests that a lateral instability associated with forced wetting disrupts the original approximately uniform flow field. Further modeling is necessary to understand the persistence of these structures.

Our argument that assumes the velocity profile is insensitive to thickness fluctuations gives a surprisingly good estimate for the gap thickness in the thin regions.

We thank Michelle Driscoll for early discussions of this work. The work was primarily supported by the University of Chicago MRSEC, funded by the National Science Foundation under Grant No. DMR-1420709 and by NSF Grant No. DMR-1404841.

[1] R. T. Perry, Fluid mechanics of entrainment through liquid-liquid and liquid-solid junctures, Ph.D. thesis, University of Minnesota, 1967.
[2] R. Burley and B. Kennedy, Chem. Eng. Sci. **31**, 901 (1976).
[3] T. Blake and K. Ruschak, Nature (London) **282**, 489 (1979).
[4] E. Vandre, M. S. Carvalho, and S. Kumar, J. Fluid Mech. **707**, 496 (2012).
[5] E. Vandre, M. Carvalho, and S. Kumar, J. Fluid Mech. **747**, 119 (2014).
[6] M. M. Driscoll and S. R. Nagel, Phys. Rev. Lett. **107**, 154502 (2011).
[7] See Supplemental Material at http://link.aps.org/supplemental/10.1103/PhysRevLett.122.018001 for details of the experimental method as well as an extended discussion of the thickness selection for the thin section of the gap.
[8] T. Tran, H. J. J. Staat, A. Prosperetti, C. Sun, and D. Lohse, Phys. Rev. Lett. **108**, 036101 (2012).
[9] R. C. A. van der Veen, T. Tran, D. Lohse, and C. Sun, Phys. Rev. E **85**, 026315 (2012).
[10] W. Bouwhuis, R. C. A. van der Veen, T. Tran, D. L. Keij, K. G. Winkels, I. R. Peters, D. van der Meer, C. Sun, J. H. Snoeijer, and D. Lohse, Phys. Rev. Lett. **109**, 264501 (2012).
[11] W. Wilkinson, Chem. Eng. Sci. **30**, 1227 (1975).
[12] E. Gutoff and C. Kendrick, AIChE J. **28**, 459 (1982).
[13] R. Burley and R. Jolly, Chem. Eng. Sci. **39**, 1357 (1984).
[14] R. Buonopane, E. Gutoff, and M. Rimore, AIChE J. **32**, 682 (1986).
[15] T. D. Blake and K. J. Ruschak, *Liquid Film Coating: Scientific Principles and Their Technological Implications*, edited by S. F. Kistler and P. M. Schweizer (Springer Netherlands, Dordrecht, 1997), pp. 63–97.
[16] A. Marchand, T. S. Chan, J. H. Snoeijer, and B. Andreotti, Phys. Rev. Lett. **108**, 204501 (2012).
[17] K. Miyamoto, Ind. Coat. Res. **1**, 71 (1991).
[18] E. Lorenceau, D. Quéré, and J. Eggers, Phys. Rev. Lett. **93**, 254501 (2004).
[19] L. D. Landau and B. V. Levich, Acta Physicochim. URSS **17**, 42 (1942).
[20] B. Derjaguin, C.R. (Dokl.) Acad. Sci. URSS **39**, 13 (1943).
[21] C. Huh and L. Scriven, J. Colloid Interface Sci. **35**, 85 (1971).
[22] Y. C. Severtson and C. K. Aidun, J. Fluid Mech. **312**, 173 (1996).
[23] Our solution for H_{thin} is not selected through curvature matching as it is in the case of deposition in the Landau-Levich-Derjaguin theory. Thus, it is not surprising that the dependence on the surface tension is different in the two cases.
[24] C. Redon, F. Brochard-Wyart, and F. Rondelez, Phys. Rev. Lett. **66**, 715 (1991).
[25] J. H. Snoeijer, G. Delon, M. Fermigier, and B. Andreotti, Phys. Rev. Lett. **96**, 174504 (2006).
[26] J. H. Snoeijer, J. Ziegler, B. Andreotti, M. Fermigier, and J. Eggers, Phys. Rev. Lett. **100**, 244502 (2008).
[27] M. Maleki, M. Reyssat, F. Restagno, D. Qur, and C. Clanet, J. Colloid Interface Sci. **354**, 359 (2011).
[28] H. E. Huppert, Nature (London) **300**, 427 (1982).
[29] S. M. Troian, E. Herbolzheimer, S. A. Safran, and J. F. Joanny, Europhys. Lett. **10**, 25 (1989).
[30] S. T. Thoroddsen and L. Mahadevan, Exp. Fluids **23**, 1 (1997).
[31] M. Rabaud, Y. Couder, and S. Michalland, Eur. J. Mech. B **10**, 253 (1991).
[32] A. Hosoi and L. Mahadevan, Phys. Fluids **11**, 97 (1999).
[33] F. Melo, J. F. Joanny, and S. Fauve, Phys. Rev. Lett. **63**, 1958 (1989).
[34] J. W. M. Bush, J. M. Aristoff, and A. E. Hosoi, J. Fluid Mech. **558**, 33 (2006).
[35] A. Oron, S. H. Davis, and S. G. Bankoff, Rev. Mod. Phys. **69**, 931 (1997).
[36] J. H. Snoeijer, B. Andreotti, G. Delon, and M. Fermigier, J. Fluid Mech. **579**, 63 (2007).
[37] G. Delon, M. Fermigier, J. H. Snoeijer, and B. Andreotti, J. Fluid Mech. **604**, 55 (2008).
[38] J. Eggers, Phys. Rev. Lett. **93**, 094502 (2004).
[39] E. Vandre, M. Carvalho, and S. Kumar, Phys. Fluids **25**, 102103 (2013).
[40] J. E. Sprittles, Phys. Rev. Lett. **118**, 114502 (2017).